

MAE C162B/C294A: Compliant Mechanism Design
Team 6 Project Report
Due: 10am on March 10th, 2022,
Los Angeles, CA

Prismatic Bearings using Compliant Mechanism Primers

Abstract

This study investigates the design of prismatic bearings using compliant mechanisms. These devices provide a single translational degree of freedom along a cylindrical axis. Variations of four different designs utilized wire, slit, and blade flexures arranged in series and parallel. Range of motion was evaluated for each design using static displacement simulations in Solidworks Simulation. The corresponding results indicate that a system consisting of a series of nested blade flexure stages axisymmetrically arranged achieves the greatest range of motion. Other designs offer different benefits at the cost of range. Further investigation of new design variations may yield potential performance improvements.

Introduction

Bearings and fasteners play a large role in the way mechanisms are designed and built. In a world that is quickly moving towards more and more mechanical automation, thanks to the growing robotic [1] and rapid layered manufacturing [2] industries, demand for more customization in mechanism design is bound to increase. This means that ‘one-size-fits-all’ solutions will likely see a decrease in popularity, at least in fields of engineering such as industrial experimentation, startups, and academic research. As shown by the rapid growth of companies such as Czinger [3], Relativity Space [4], and Harvest Automation [5], which directly take advantage of cutting-edge, highly customized technologies, innovation is commonly paired with a high level of customization. In many cases, this is made complicated (or even impossible) through standardized connectors such as bearings.

For designs where performance and precision are of utmost importance, ‘standard’ bearings and connectors generally do not suffice, and the alternative solutions are to either outsource ‘performance parts’, as many Formula 1 racing teams do [6], or to build bespoke parts in-house. The focus of this report is on the latter strategy, and, more specifically, the making of prismatic bearings that allow for translation in a specific direction with a set range of motion.

Oftentimes, as shown by companies like Airbus [7], the best alternative when it comes to design optimization is to replace assemblies with one-part counterparts, so that design requirements can be more finely tuned for a specific problem. With regards to the making of prismatic bearings, the goal of this study is to showcase various methods to achieve fixed-range translating motion using compliant mechanisms that replace the traditional means of making things move in a straight line.

The introduction of *compliant* mechanisms over the past two decades has been a game changer in the field of precision engineering, as they are immune (in theory) to issues such as wear, friction, and clearance. They have demonstrated usage in a host of applications including Soft Robotics [8] and even the thermal characterization of a skin where compliance of the actuator was able to adapt to the compliance of human skin [9].

With relation to compliant mechanisms, a host of researchers have designed various mechanisms with the objective of generating multiple translations using flexures. For instance, a compliant positioning mechanism for a piezoelectric actuator has a compound decoupling guide mechanism which results in a cross axis coupling ratio below 0.6% and a positioning resolution of 10 nm [10]. Compliant mechanisms were also used to produce 3 directional translational motion [11], large range XY translational motion with enhanced out of plane stiffness[12], 3PUU(Prismatic Universal Universal) micromanipulators for nanomanipulation [13] with a specified travel range for high payload capacity[14], and flexure based joint chains for two translations[15].

With regards to the task of achieving a single translating motion, though, there is a lot of prior literature.

The work of J. Wang et al. with regards to designing a vibrating module for laser machining [16] led to a design that uses curved blade flexures arranged in a cylinder to produce motion along the axis of the cylinder, as shown in Figure 1.

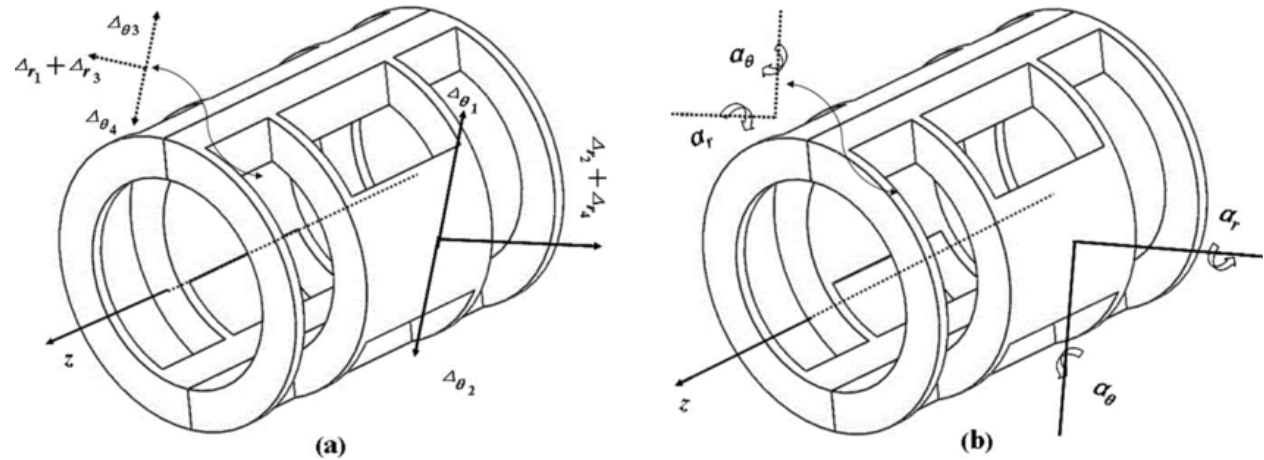


Figure 1. Design for a module in laser machining that employs compliance [16].

Work by M. Tellaria [17] [18] led to the formulation of a design paradigm specifically targeted to the design of cylindrical flexures, which led to many successful designs, such as the one shown in Figure 2, which can achieve planar translation and rotation.

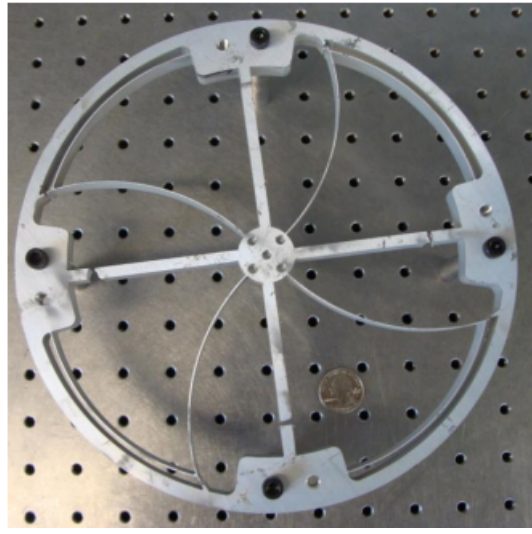


Figure 2. Cylindrical flexure capable of planar translation and rotation (X, Y, Θ_z) [17].

Work by L. Howell et al. [19][20][21] led to the formulation of designs that take advantage of serial blade flexures in double shear to obtain translating motion from a flat sheet, as shown in Figure 3.

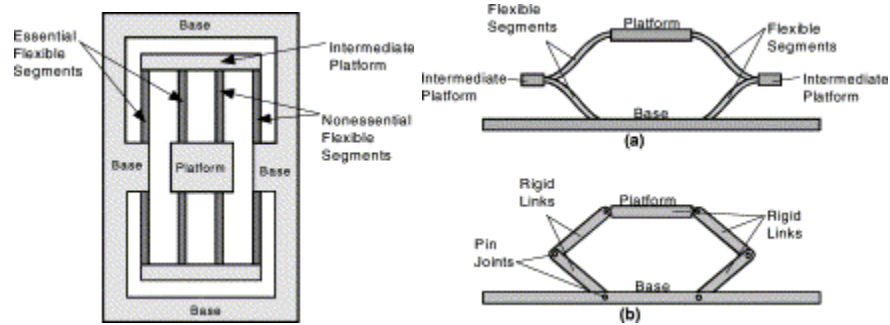


Figure 3. Translating flexure obtained using pseudo-rigid model[19,20].

A manipulator designed by T.J. Teo et al. [22] is made out of three parallel compliant mechanisms able to achieve translation to control the orientation of a connected platform, as shown in Figure 4.

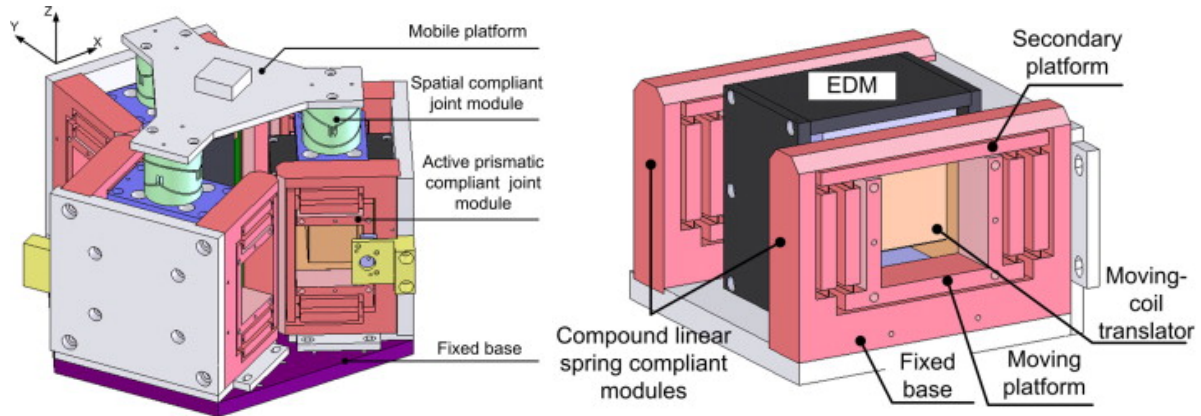


Figure 4. Compliant prismatic modules used in movable platform design [22].

By creating compliant versions of known n-bar linkages able to synthesize translation, Pavlovic and Pavlovic [23] have recreated planar guides such as the one presented in Figure 5.

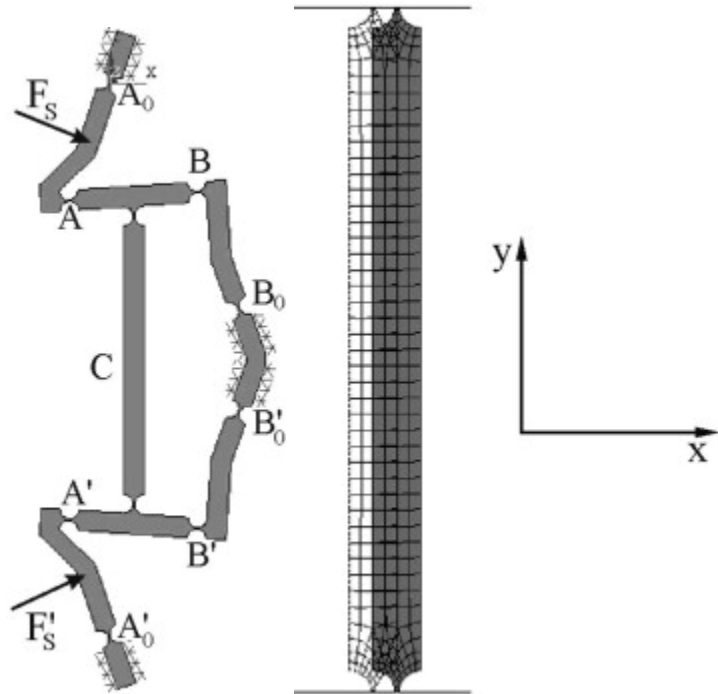


Figure 5. Translating mechanism obtained by replacing revolutes in parallel mechanism with notch flexures [23].

Work by B. P. Trease on large displacement compliant joints [24] includes a single translation design, shown in Figure 6, that can be used both in parallel and in series for different outcomes.

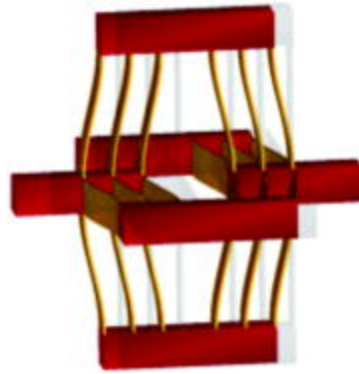


Figure 6. Translating flexure system designed for high displacement [24].

When compiling a literature survey of the FACT design approach, Macheckposhti et al. [25] include a list of feasible designs for simple translating motion, presented in Figure 7.

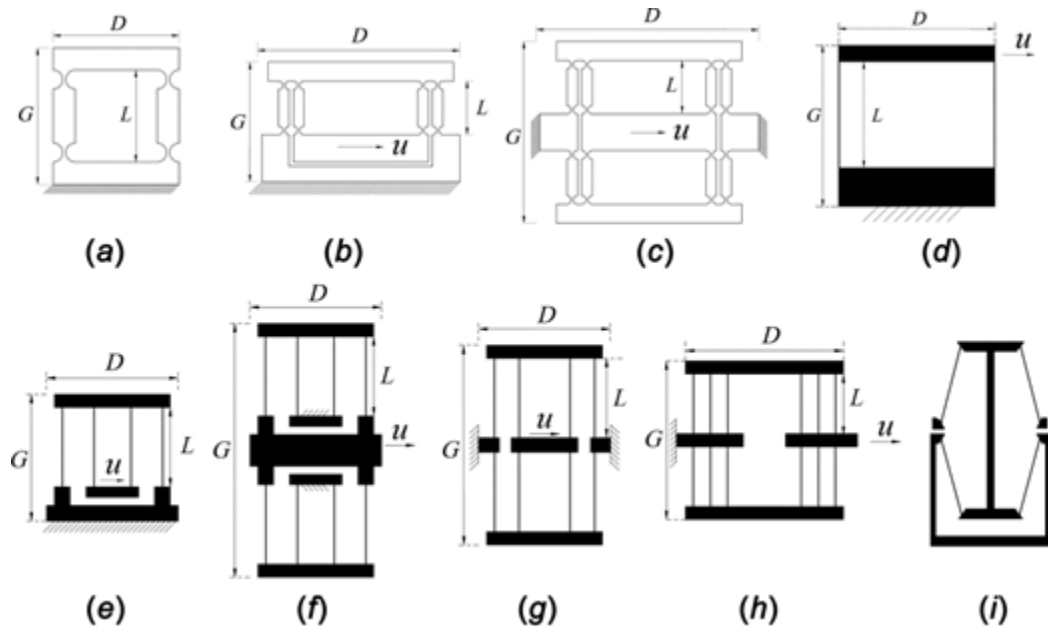


Figure 7. List of flexure designs capable of translating motion obtained from FACT library [25].

2. Materials and Methods

Overview: In this study, four designs were analyzed: diaphragm, symmetric, axisymmetric, and parallel. Each design achieves one translational degree of freedom via at least two parallel constraint planes separated by some nonzero distance.

2.a. Diaphragm

The three diaphragm designs studied in this project all revolve around the concept of using flexures that lie on the same plane to achieve perpendicular translation. Thanks to this configuration, they can be manufactured into circular diaphragms and strategically placed along a given prismatic joint to constrain motion. Due to their planar nature, these flexures have a somewhat limited range of motion, but they are versatile (in terms of installation into existing assemblies) due to their simplicity.

Figure 8 shows the three designs studied here. The first one, the wire diaphragm design, uses ten wire flexures, located in such a way that they are all tangent to a common circumference, to form a 3 degrees-of-freedom mechanism that is overconstrained by 7. The second one, the curved blade diaphragm design, replaces the wire flexures with curved blades while retaining the same 3 degrees of freedom. (Curved blades are stronger than thin wire flexures while still retaining the same motion.) The third and last design, the slit series design, consists of a serial element with four C-shaped slits that allow for the structure to deform, similar to a kirigami pyramid structure [<https://wulixb.iphy.ac.cn/en/article/doi/10.7498/aps.69.20200112>].

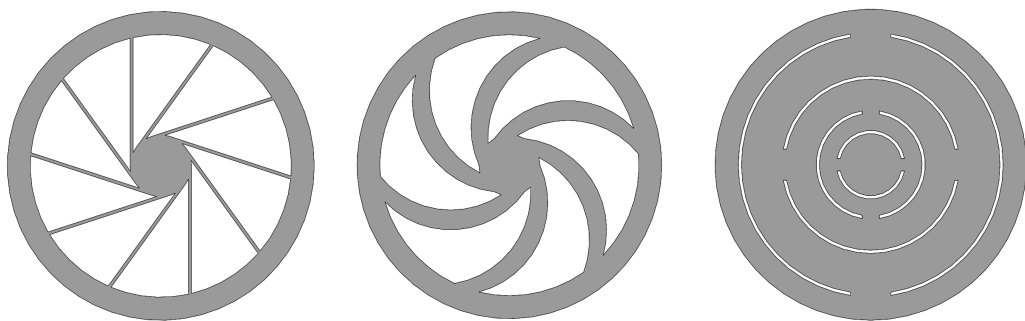


Figure 8. Diaphragm design using (left) wire flexures, (middle) curved blade flexures, and (right) slits.

All designs allow for the motion of the center circle relative to the outer disk, with a translation perpendicular to the diaphragm plane. Rotations are also present, but since at least two diaphragms are used to construct the prismatic bearing, these other motions are constrained in the final assembly.

2.b. Axisymmetric

Axisymmetric designs take advantage of repeated serial flexure limbs located on a cylindrical shell of constant width, as shown in figure 9. A ground is connected to a stage through a series of curved horizontal blade flexures and intermediate stages. To obtain a full 360° cylinder, these modules are axisymmetrically repeated.

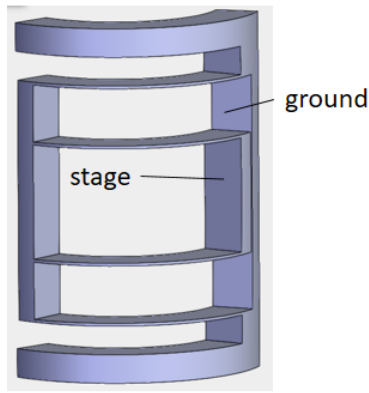


Figure 9. Single flexure sector used in axisymmetric design.

Three design parameters can be changed in the axisymmetric design: number of flexures, number of sectors, and number of nestings.

Number of flexures refers to the number of parallel curved blade flexures between each rigid body. Figure 10 shows how two components in the flexure system can be connected by a different number of blades. More blades will increase the stiffness of the structure without changing the range.

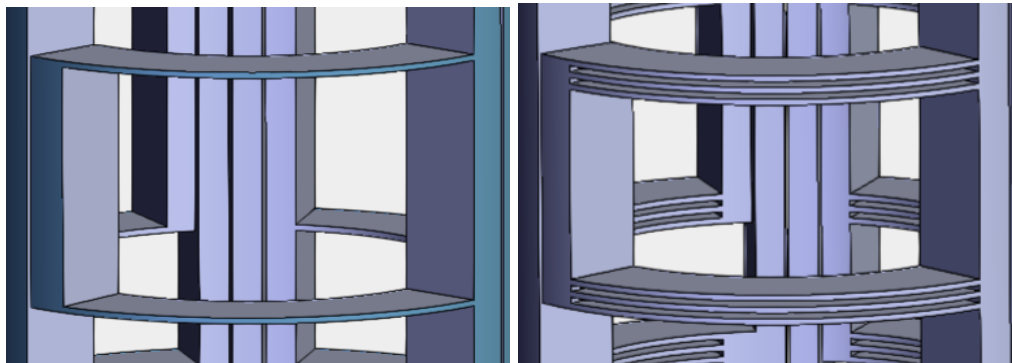


Figure 10. Axisymmetric design with (left) one flexure and (right) three flexures.

Number of sectors refers to the number of times the section presented in Figure 9 is used to ‘fill’ 360° . Figure 11 showcases designs with differing numbers of sectors. If two sectors are desired, for example, each will measure 180° , while if five are desired, each will be 72° . Increasing the number of sectors improves the structural rigidity of the cylindrical ground. However, this also decreases the overall range because the arc length of each flexure decreases. Figure 11 illustrates how increasing the number of sectors increases the number of vertical beams connecting the top and bottom ground bodies while also drastically decreasing the flexure arc length.

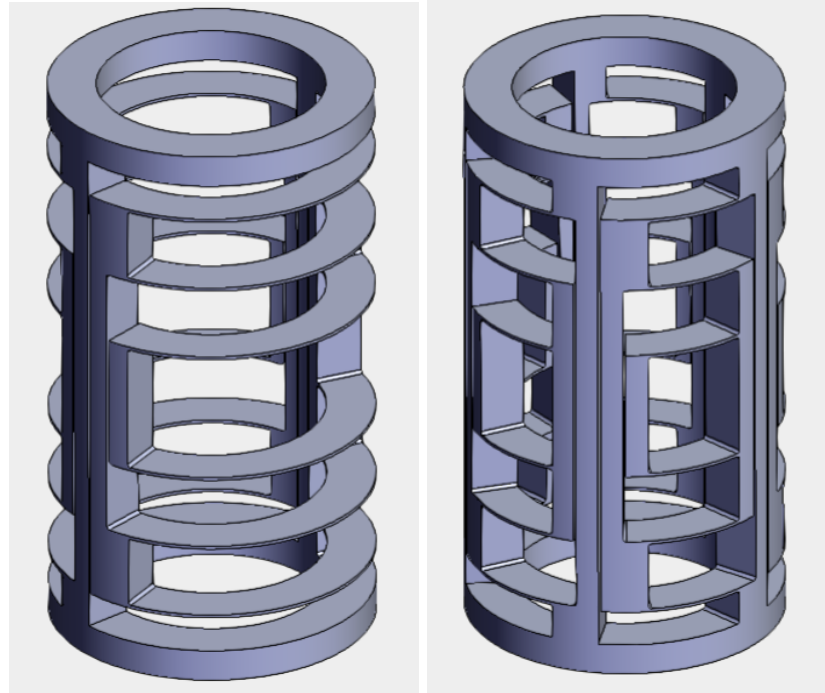


Figure 11. Axisymmetric design with (left) two sectors and (right) three sectors.

Number of nestings describes the number of flexures and stages in series. Flexures with differing numbers of nestings are shown in Figure 12, where the design on the left is only nested one time, while the one on the right is nested six times. It should be noted that the overall height of the cylinders does not necessarily depend on the number of nestings, and that it is also affected by the r value for the blades, as presented in the simulation section.

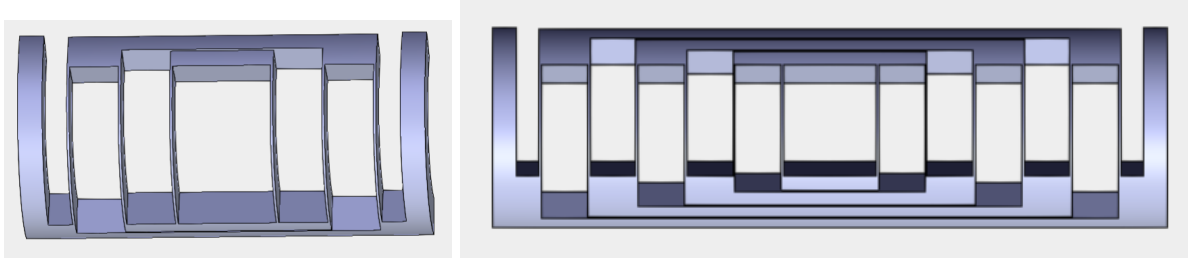


Figure 12. Axisymmetric sector with (left) three nestings and (right) six nestings.

2.c. Symmetric

Working similarly to the axisymmetric design, the symmetric design takes advantage of the same serial arrangement of curved blade flexures, but uses a different scheme to combine them and ‘fill the cylinder’. While the former repeats the limbs, the latter mirrors them, producing a structure with twice as many symmetry planes. For example, Figure 13 illustrates half of one symmetric sector with three nestings for the 3 sector symmetric design. To ‘fill the cylinder’, this half-sector was mirrored vertically, copied three times axisymmetrically, and then mirrored horizontally.

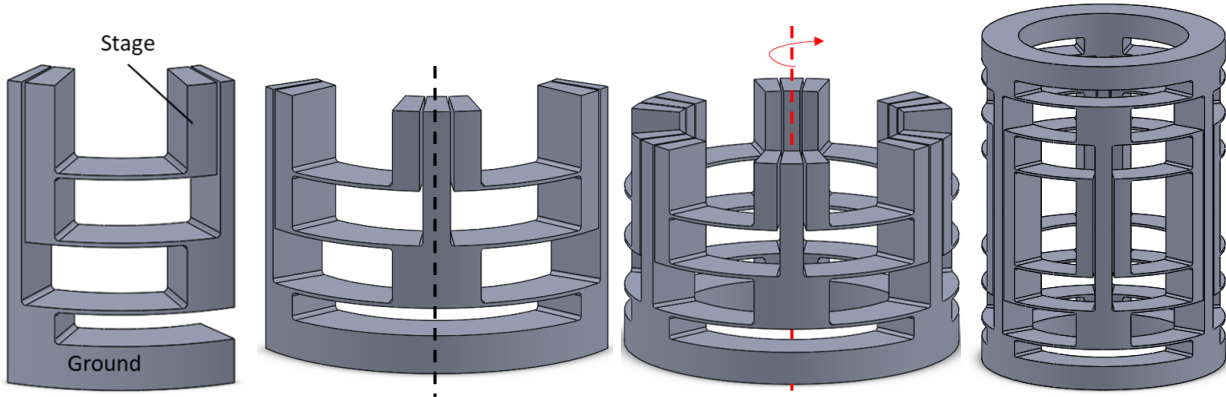


Figure 13. (first) Half sector, (second) symmetric sector, (third) three repeated sectors, (fourth) full cylinder.

Similar to axisymmetric, the variable design parameters for this scheme include number of nestings, number of flexures, and number of sectors. Given the similarity of the axisymmetric and symmetric designs, only a variable number of symmetric sectors was investigated. Figure 14 shows a symmetric design with two and five sector.

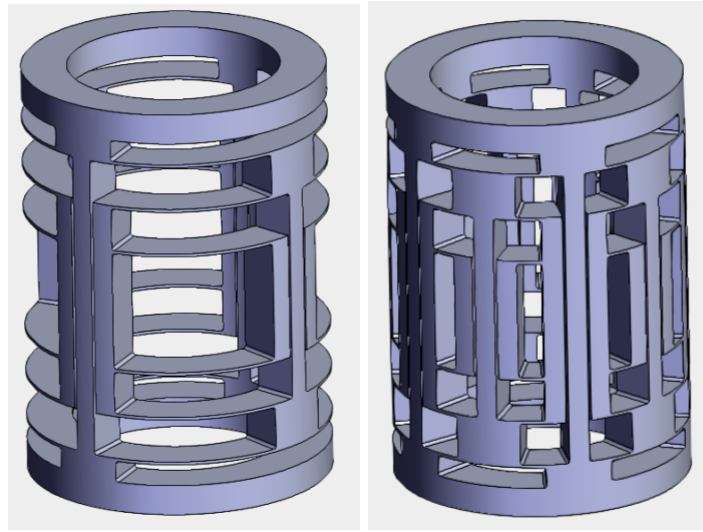


Figure 14. Symmetric design with (left) Two and (right) five sectors.

2.d. Parallel

Unlike the axisymmetric and symmetric designs, the parallel design does not contain intermediate bodies. Figure 15 shows one sector of the first parallel design which consisted of five horizontal blade flexures connecting the ground and stage. Three identical sectors were arranged axisymmetrically to form the final design. This parallel design utilizes the same working principles as the previous serial designs albeit with less range due to the lack of serial nestings. Consequently, it has similar design parameters, namely variable number of sectors and flexures. Changing these parameters would result in similar design variations.

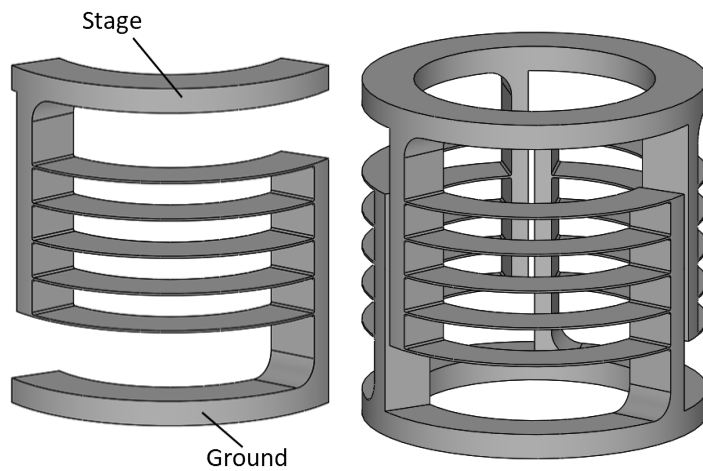


Figure 15. (left) One sector and (right) full assembly of the first parallel design.

Figure 16 illustrates one sector of the second parallel design. Unlike the first design, two serial blade flexure elements consisting of one vertical and one oblique blade flexure are arranged in parallel between the ground and stage. In this case, each serial blade flexure acts as a single pure force constraint located at the vertex of each serial element oriented along its seam. The final design shown in Figure 16 possesses two horizontal constraint planes each having three constraint lines that don't all intersect at the same point. As a result, a vertical translation was the only permissible motion.

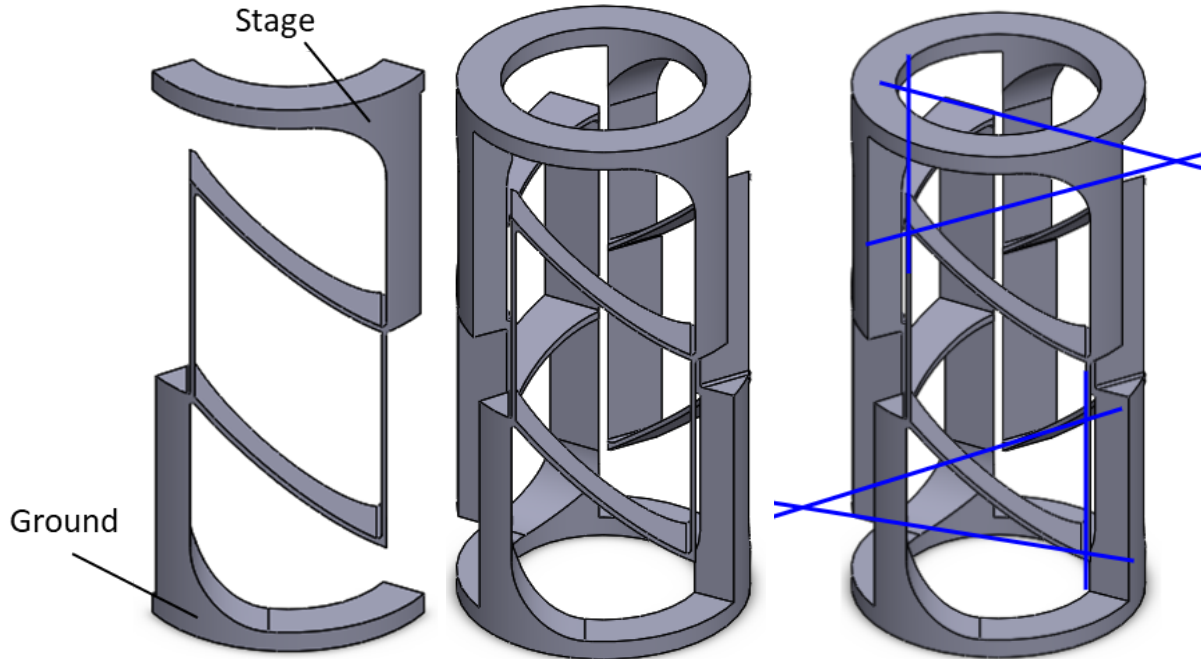


Figure 16. (left) One sector, (middle) full assembly, and (right) constraint space of the parallel design.

Although no variations of the second parallel design were investigated, there are many parameters that may be changed to generate new models. For any given number of sectors, changing the flexure lengths in each serial element will result in change of stiffness and range. The gaps between the vertices of each serial element and the ground and stage can then be changed accordingly in order to prevent yielding.

3. Simulations

All simulations were conducted using Solidworks Simulation Tool. Material properties of 20% infill PLA [26-29] were used for the simulations.

3.a. Diaphragm Optimization

To begin, we chose in-plane symmetric diaphragm designs, which eliminate the possibility of in-plane movement of the system. We performed shape optimization on the diaphragm design to ensure maximum displacement along the z-axis. The optimization set-up is shown in Figure 17. Parameters r_1 and r_2 describe the distances between the two-middle c-shaped slits, and are varied as the innermost and outermost slits are kept in the same position to ensure the diaphragm is properly mated to the rest of the assembly.

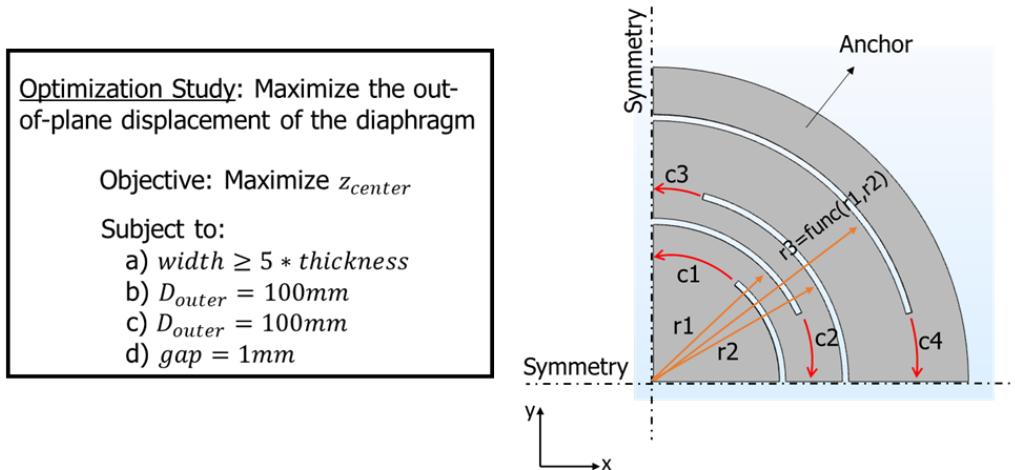


Figure 17. Shape optimization of serial-slit diaphragm design (left). A quarter-symmetric serial design with optimization parameters r_1 and r_2 (right).

Along with optimization study, a finite element analysis is also conducted to figure out the optimal displacement-to-stress ratio. In this study, a point load is applied at the center of the diaphragm design which is kept fixed along the periphery. The diaphragm design along with boundary conditions are shown in Figure 18.

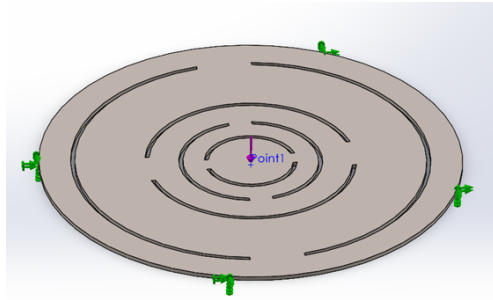


Figure 18. Forces (purple) and constraints (green) used in diaphragm topology optimization.

3.b. Axisymmetric, Symmetric, and Parallel Optimization

For the serial and parallel blade flexure designs, a static displacement simulation was performed to determine total range, R. Figure 19 shows the simulation setups consisting of fixtures applied to the ground elements and prescribed vertical displacements applied to various platforms. For a single blade flexure, the displacement was applied to a horizontal surface to prevent any rotation of the stage. For the symmetric and axisymmetric designs, the central shaft was displaced. Contacts between the central shaft and the stages were set as perfect bonds. The stage of the parallel designs was directly displaced.

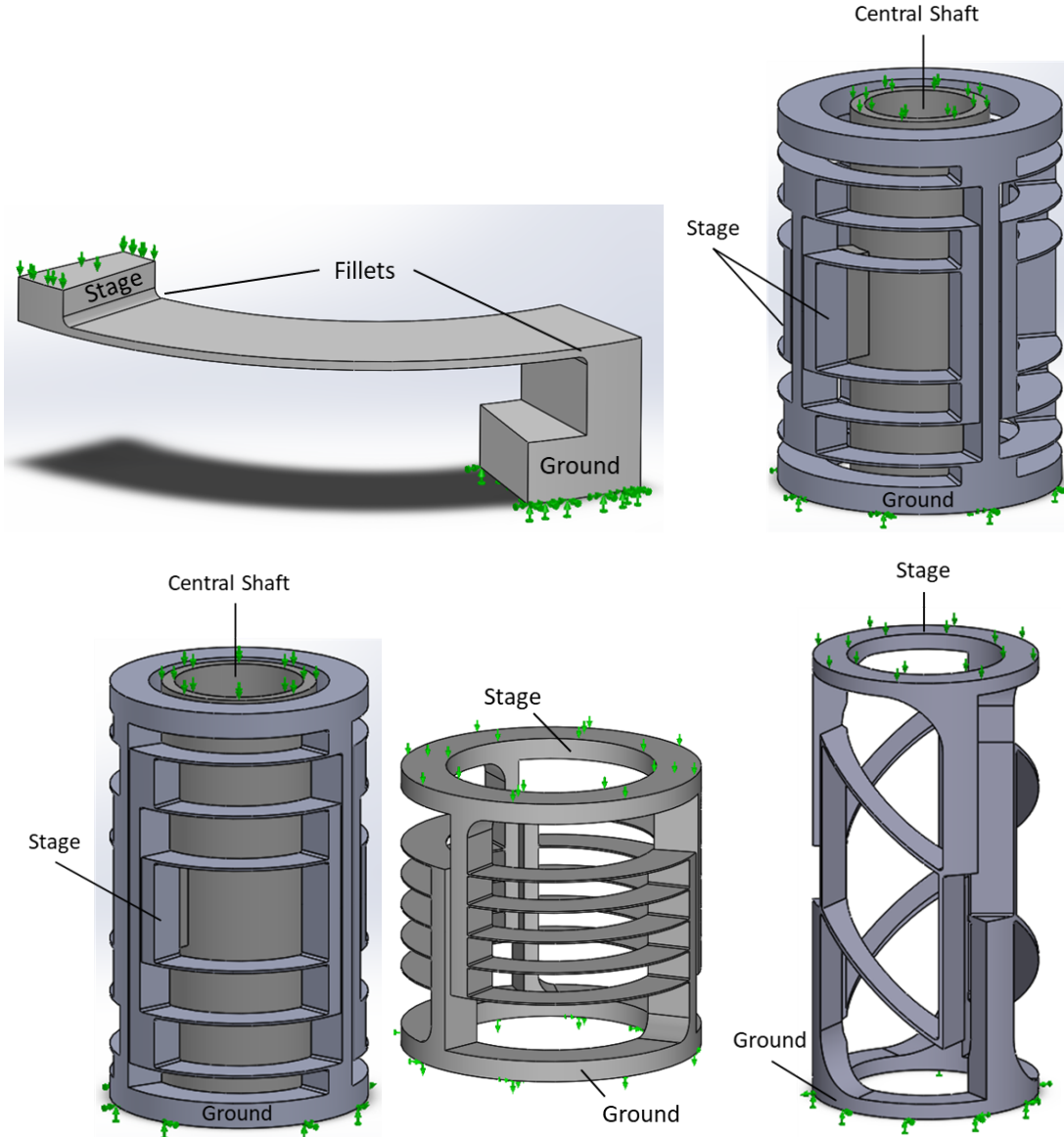


Figure 19. Simulation setups for the (top left) single flexure, (top right) symmetric, (bottom left) axisymmetric, and (bottom middle/right) parallel designs.

Once set up, each system underwent the same test procedures. First, a coarse mesh was generated with the smallest element dimension equalling half the flexure thickness. The mesh was then refined in a series of h-adaptive iterations. In this automated process, von mises stress distribution results were used to refine the mesh in areas of high stress and coarsen the mesh in areas of low stress. Mesh refinement was then repeated until a refined mesh with 98% confidence was achieved. Figure 20 illustrates one of the final mesh distributions achieved using

h-adaptive mesh refinement. Lastly, the displacement magnitude was adjusted until the maximum von mises stress was equal to 80% of the yield strength.

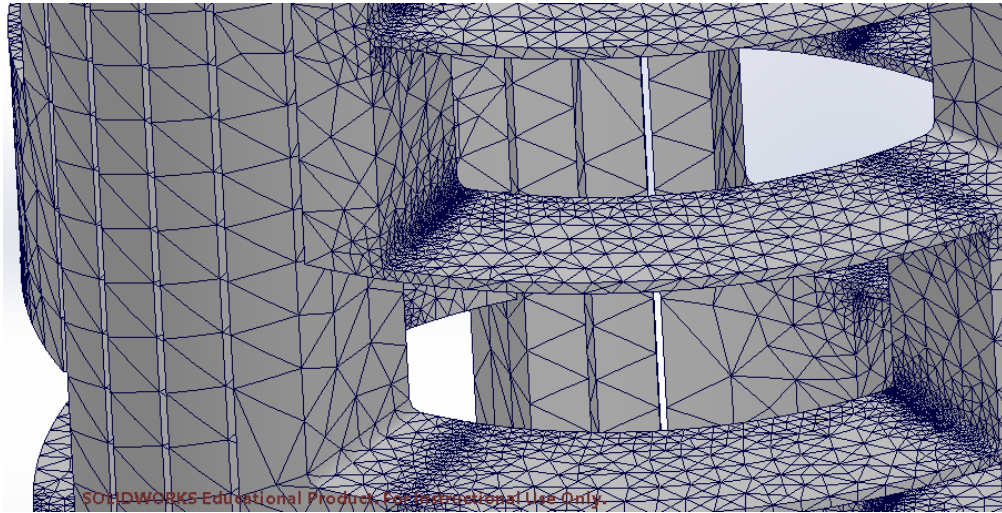


Figure 20. An example of h-adaptive mesh refinement result.

3.c. Blade Flexures Radius

Since perfect corners produce an infinite stress concentration factor, the mesh refinement process resulted in an endless loop. This was remedied by adding a fillet with a nonzero radius to all corners formed by blade flexures. Figure 21 illustrates the relationship between normalized range of motion and fillet radius for a 1mm thick blade flexure. Displacement simulations were performed on the single flexure model with a fillet radius ranging from 0.1mm to 2mm. A 1mm fillet radius was chosen due to the rapidly diminishing increase in range with increasing fillet radius.

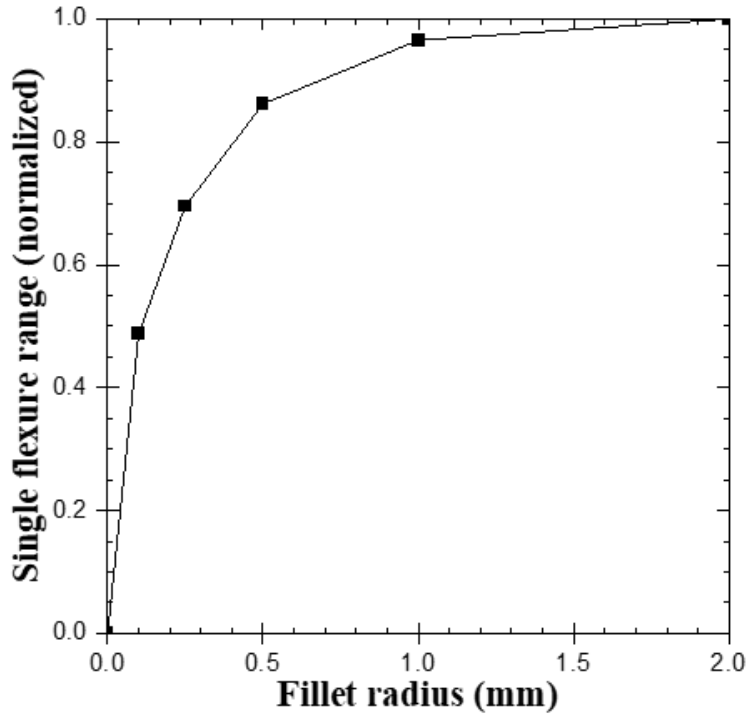


Figure 21. Single flexure range as a function of fillet radius.

4. Results and Conclusion

4.a. Diaphragm

The result from the optimization study done on serial-slit-design confirms that the serial-slit-design having minimum achievable width for the outermost nesting provides optimal result. In other words, optimal diaphragm design is obtained when parameters r_1 and r_2 are maximized. The optimized serial-slit design is shown in Figure 22.

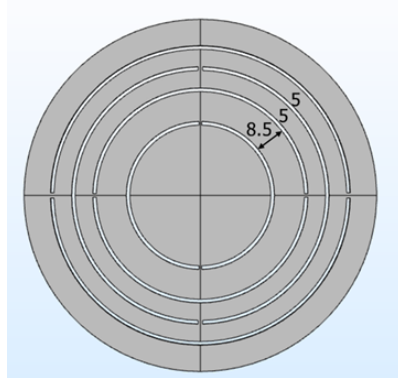


Figure 22. Optimized series slit diaphragm design

Results of the finite element study done on the slit series diaphragm design are presented in Figure 23, where maximum stress, maximum displacement, and the ratio between them, as a measure of performance, are presented for each combination of r_1 and r_2 within a set design space. For each plot, a red X is used to mark the most ‘optimal’ design, according to the ratio performance metric.

As it can be seen, the highest displacement to stress ratio is obtained if both r_1 and r_2 are maximized. This is a somewhat obvious result, since it confirms that deflection is maximized by minimizing the cross sectional area of each intermediate component of the flexure.

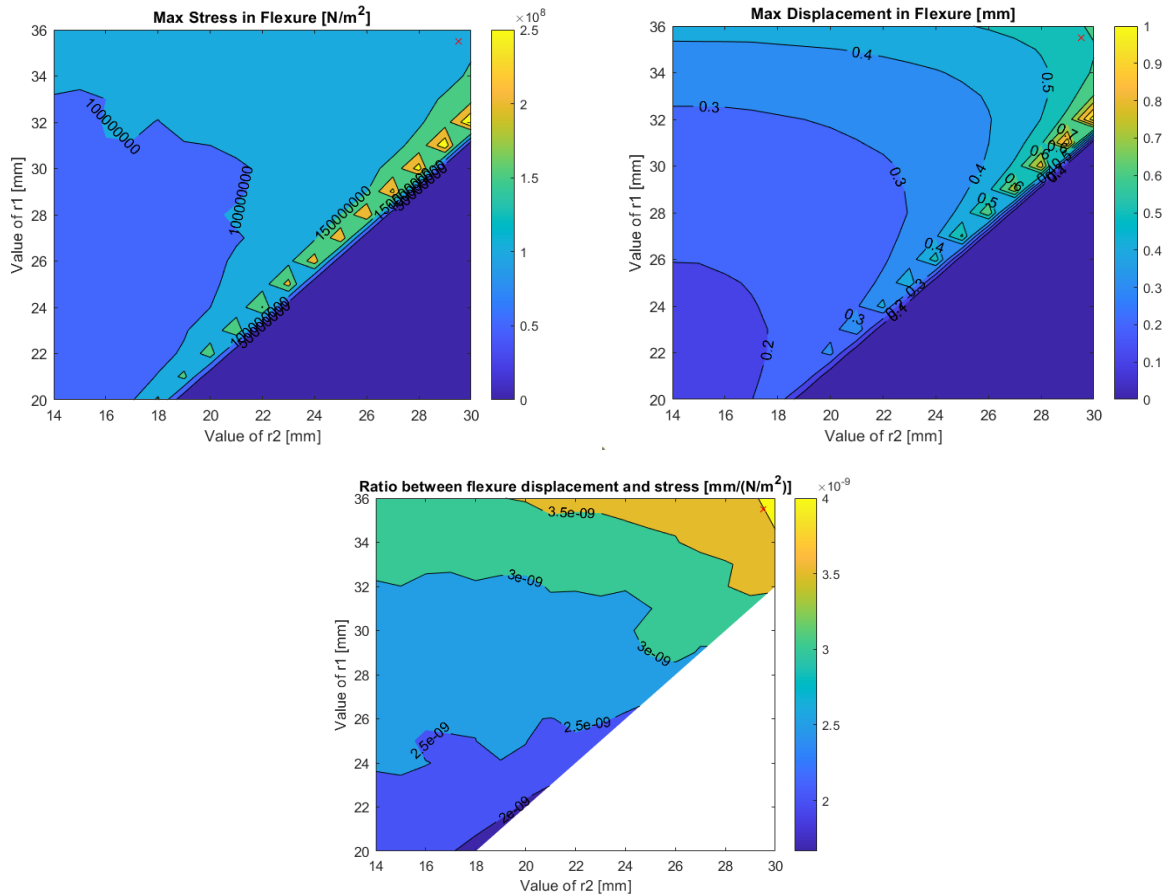


Figure 23. Plots of maximum internal stress (top left), maximum displacement (top right), and ratio between them (bottom) from topology optimization.

Given the fact that the optimization study led to the conclusion that displacement would be maximized by minimizing width, in order to propagate this effect, the design was modified to include an additional slit, raising the number from four to five, such that the distance between them would be minimized to 5.1 mm, as shown in Figure 24.



Figure 24. Modified series slit diaphragm design after topology optimization study.

For all diaphragm designs, snap fit connections were added to connect them to an outer cylindrical ‘ground’ and an inner ‘stage’. The snap fit connection consisted of holes that were placed on the ‘ground’ and ‘stage’ and knobs on the diaphragm. The clearance between the holes and knobs were designed to be 0.1mm, considering the precision of the 3D printer used: Prusa i3 MK3S+ (Prusa) with PLA filament. Specifically, diameters of holes on the ‘ground’ and ‘stage’ were designed to be 4.5mm and 15mm, respectively. Additionally, chamfers were added on the top of each holes and knobs to facilitate assembling the parts. Angle and depth of the chamfers on the holes were set to 60° and 0.5mm, respectively. Counterparts on the knobs were in 60° and 1mm. For the ground, a mesh was created to aid the view of the motion of the inner stage. The final designs were 3D-printed using Prusa, and each design is shown in Figure 25.

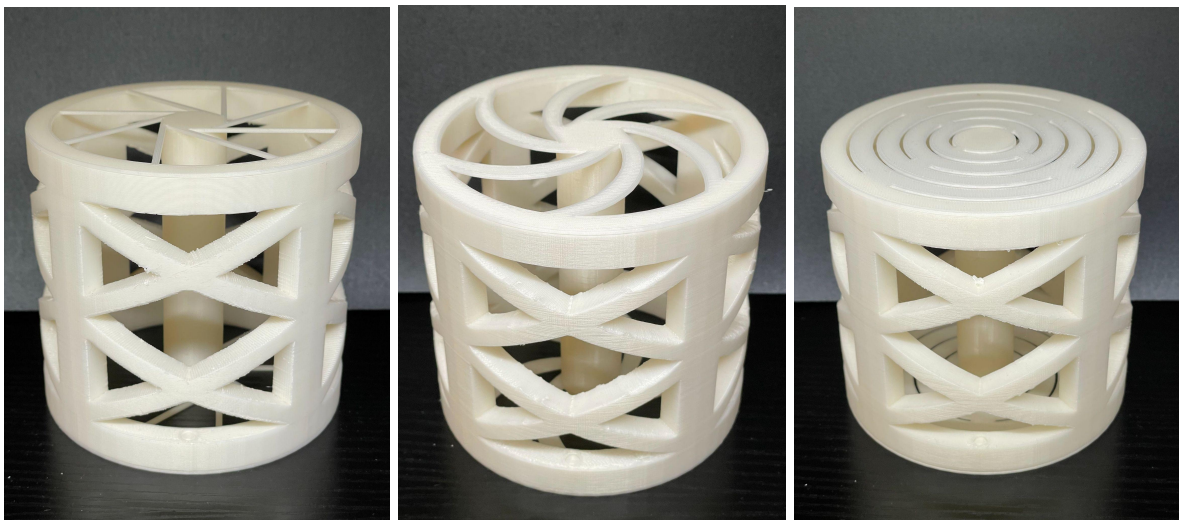


Figure 25. Printed designs for each diaphragm type.

4.b. Axisymmetric

Figure 26 shows the single flexure range r and total range R as a function of number of nestings N , as well as the predicted total range based on single flexure range ($N \times r$). All curves intersect at $N = 1$ since a system with one nesting has the same range as a single flexure. Similarly, both simulated and predicted total range approach zero as the flexure range decreases to zero at $N = 13$. The single flexure and full assembly simulations predict a maximum total range of 40.0 mm and 38.2 mm, respectively.

The disagreement between single flexure and full assembly simulations can be attributed to the difference in mesh quality between the two models. The single flexure simulations achieved a finer mesh since the single flexure model is smaller than the full assembly. As N increases, the size of the full assembly increases, leading to a coarser mesh relative to the model size. As a result, the range discrepancy between single flexure and full assembly results to increase with increasing N , as shown in Figure 26.

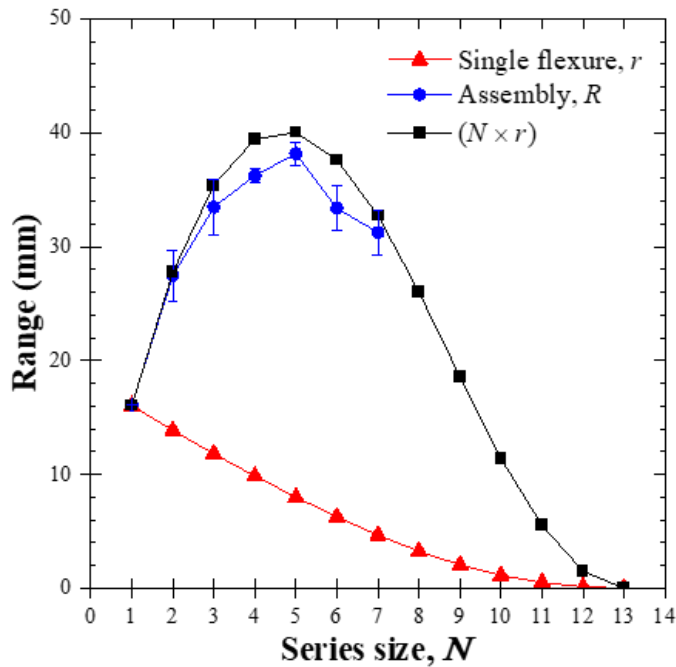


Figure 26. Single flexure range r and total range R as a function of number of nestings N . The total range agrees with the predicted range based on single flexure simulations ($N \times r$).

The axisymmetric design with 3 nestings ($N = 3$) was selected to be printed. In the final design, the outer cylinder consisting of the “ground” and the nestings was printed as a separate part, while the central shaft with extrusions was printed as another. Same Prusa with PLA setting in the diaphragm manufacture was used here. The central shaft was subsequently glued to the

center nesting (or the “stage”) with Gorilla Super Glue Gel 20g. Figure 27 shows the printed and manufactured axisymmetric design.

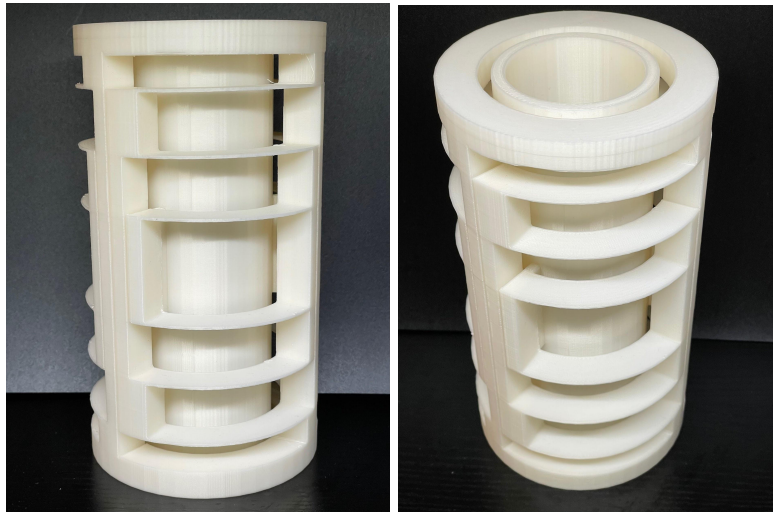


Figure 27. Printed axisymmetric design.

4.c. Symmetric

The symmetric design with 2 nestings ($N = 2$) was selected to be printed. In the final design, the outer cylinder consisting of the “ground” and the nestings were printed as a separate part, while the central shaft with extrusions was printed as another. Same Prusa with PLA setting in the diaphragm and axisymmetric manufacture was used here. The central shaft was subsequently glued to the center nesting (or the “stage”) with Gorilla Super Glue Gel 20g. Figure 28 shows the printed and manufactured symmetric design.



Figure 28. Printed symmetric design.

4.d. Parallel

The parallel design with three sectors was selected to be printed. The entire assembly was printed whole using the same Prusa printer and PLA filament with full supports. Figure 29 shows the final print result after support removal.



Figure 29. First printed parallel design.

The second parallel design with three sectors was selected to be printed. Since the flexure blades don't lie on the x-y plane, printing the full assembly upright in short filament fibers perpendicular to the length of each flexure blade. Instead, each sector was printed separately in a horizontal configuration with full supports. The three sectors were subsequently glued together using Gorilla Super Glue Gel 20g. Figure 30 displays one sector and three glued sectors prints.



Figure 30. (left) One sector and (middle/right) full cylinder of second parallel design.

In conclusion, the axisymmetric design provides the most range of motion with five nestings and reasonable structure rigidity with three sectors. For a given number of sectors, the symmetric design achieves approximately half as much range as the axisymmetric design while doubling the structural integrity of the cylinder. While the parallel designs in this study achieved comparable ranges to the serial designs, further investigation of design variations may lead to significant range improvement. The diaphragm designs have much smaller ranges but allow for more design customization since each diaphragm is an independent component.

Contributions

- **Ren, Ruoning:** *Axisymmetric* - CAD adjustments, FEA simulation of varied nestings (N1 to N7), analysis
- **Rivera, Ryan Jared:** *Manuscript* - writing and editing
- **Sainaghi, Pietro:** *Diaphragm* - simulation, CAD for slit series, design modifications for slit series, printed parts, *Axisymmetric* - Simulation, normalization of cads, printed parts, *Symmetric* - printed parts, *Manuscript* - literature review, writing and editing, *Project Management*
- **Samaan, Fadi:** *Axisymmetric* - CAD/design, simulation, analysis, *Symmetric* - CAD/design, simulation, *Parallel* - CAD/design, simulation, printing, *Manuscript* - writing, editing, data curation, *Presentation* - writing, editing, *Project Management*.
- **Sanghai, Nikunj:** *Research*: Different 1 DOF systems , *Manuscript*- Introduction, Literature Review, Writing & Editing
- **Sharma, Vaibhav:** *Diaphragm*- optimization & simulations, *Manuscript* - writing and editing
- **Shi, Huangshuai:** *Axisymmetric* - simulation, CAD editing
- **Thapa, Dipesh:** *Diaphragm*- Early optimization runs, *Research*- mechanisms
- **Uribe, Rodrigo**
- **Nieman, Christian Alexander:** *Symmetric* - CAD, *Manuscript* - editing
- **Rabbani, Mateen Ali:** *Axisymmetric* - CAD and design of all varied nestings, varied flexures, and varied sectors, *Symmetric* - CAD adjustments, *Presentation* - writing and editing
- **Reedel, Brandon John**
- **Rossmango, Ryan John:** *Axisymmetric* - CAD models of 3 Nesting Varying Flexures, made test print of simplified axisymm model; *Project management* - organized team Discord, assigned clear roles; *Presentation* - writing and editing
- **Saavedra Garcia, Eric Eduardo:** *Diaphragm* - Simulations, Designed Outer cylinder with windows, *Axisymmetric* - 3 Nesting (3&2 flexures) edits, *Project Management* - Lead presentations on thursdays, collected initial CAD files

- **Sanghavi Vedha**: *Research* for different mechanisms, *Manuscript* - writing and editing
- **Santora, Dylan Matthew**: *Manuscript* - writing and editing
- **Sefkow, Conor Joseph**: *Manuscript* - writing and editing
- **Song, Zhantao**: *Diaphragm* - simulation, CAD for press fits, wire diaphragm modification, printed parts, *Axisymmetric* - assembling, *Symmetric* - assembling, *Manuscript* - writing and editing
- **Spycher, Luca Fred**: *Symmetric* - symmetric halves CAD, *Manuscript* - editing and a little preliminary research

Bibliography

[1]

M. Teulieres, J. Tilley, “Industrial Robotics, Insight Into the Sector’s Future Growth Dynamics,” *McKinsey & Company*, July 2019.

<https://www.mckinsey.com/~/media/mckinsey/industries/advanced%20electronics/our%20insights/growth%20dynamics%20in%20industrial%20robotics/industrial-robotics-insights-into-the-sectors-future-growth-dynamics.ashx>

[2]

“Wohlers Report 2021”. Wohlers Associates(2021).

<https://wohlersassociates.com/2021report.htm>

[3]

Czinger Website.

<https://www.czinger.com/>

[4]

Relativity Space Website.

<https://www.relativityspace.com/>

[5]

Harvest Automation Website.

<https://www.public.harvestai.com/>

[6]

T. Chachra, “F1 Engine suppliers 2020: Who supplies engines to Formula 1 teams?,” *The SportsRush*, Aug. 16, 2020.

<https://thesportsrush.com/f1-news-f1-engine-suppliers-2020-who-supplies-engines-to-formula-1-teams/>

[7]

M. Tomlin and J. Meyer, “Topology Optimization of an Additive Layer Manufactured (ALM) Aerospace Part,” p. 9, 2011.

<https://www.mmsonline.com/cdn/cms/uploadedFiles/Topology-Optimization-of-an-Additive-Layer-Manufactured-Aerospace-Part.pdf>

[8]

D. Rus and M. T. Tolley, “Design, fabrication and control of soft robots,” *Nature*, vol. 521, no. 7553, Art. no. 7553, May 2015, doi: [10.1038/nature14543](https://doi.org/10.1038/nature14543).

[9]

R. C. Webb *et al.*, “Ultrathin conformal devices for precise and continuous thermal characterization of human skin,” *Nature Mater*, vol. 12, no. 10, Art. no. 10, Oct. 2013, doi: [10.1038/nmat3755](https://doi.org/10.1038/nmat3755).

[10]

F. Wang *et al.*, “A 2-DOF nano-positioning scanner with novel compound decoupling-guiding mechanism,” *Mechanism and Machine Theory*, vol. 155, p. 104066, Jan. 2021, doi: [10.1016/j.mechmachtheory.2020.104066](https://doi.org/10.1016/j.mechmachtheory.2020.104066).

[11]

G. Hao and X. Kong, “Design and Modeling of a Large-Range Modular XYZ Compliant Parallel Manipulator Using Identical Spatial Modules,” 2012, doi: [10.1115/1.4006188](https://doi.org/10.1115/1.4006188).

[12]

G. Hao and X. Kong, “A Novel Large-Range XY Compliant Parallel Manipulator With Enhanced Out-of-Plane Stiffness,” *Journal of Mechanical Design*, vol. 134, no. 6, May 2012, doi: [10.1115/1.4006653](https://doi.org/10.1115/1.4006653).

[13]

Y. Li and Q. Xu, “Novel Design of a 3-PUU Spatial Compliant Parallel Micromanipulator for Nanomanipulation*.” 2005.

<https://citeseerx.ist.psu.edu/viewdoc/download?doi=10.1.1.702.7222&rep=rep1&type=pdf>

[14]

S. Fan, H. Liu, and D. Fan, “Design and development of a novel monolithic compliant XY stage with centimeter travel range and high payload capacity,” *Mech. Sci.*, vol. 9, no. 1, pp. 161–176, Mar. 2018, doi: [10.5194/ms-9-161-2018](https://doi.org/10.5194/ms-9-161-2018).

[15]

K.-B. Choi, J. Lee, G. Kim, and H. Lim, “A Compliant Parallel Mechanism with Flexure-based Joint Chains for Two Translations,” *International Journal of Precision Engineering and Manufacturing*, vol. 13, Sep. 2012, doi: [10.1007/s12541-012-0213-1](https://doi.org/10.1007/s12541-012-0213-1).

[16]

J. Wang, S. Jang, E. Kim, Y. Jeon, S.-H. Lee, and M. Lee, “Design and verification of a novel hollow vibrating module for laser machining,” *The Review of scientific instruments*, vol. 86, p. 045104, Apr. 2015, doi: [10.1063/1.4918618](https://doi.org/10.1063/1.4918618).

[17]

M. J. Telleria, “Design Rules and Models for the Synthesis and Optimization of Cylindrical Flexures,” p. 210.

<https://dspace.mit.edu/bitstream/handle/1721.1/81755/860983395-MIT.pdf;sequence=2>

[18]

M. J. Telleria and M. L. Culpepper, “Understanding the drivers for the development of design rules for the synthesis of cylindrical flexures,” *Mechanical Sciences*, vol. 3, no. 1, pp. 25–32, Apr. 2012, doi: [10.5194/ms-3-25-2012](https://doi.org/10.5194/ms-3-25-2012).

[19]

D. L. Wilcox and L. L. Howell, “Fully compliant tensural bistable micromechanisms (FTBM),” *Journal of Microelectromechanical Systems*, vol. 14, no. 6, pp. 1223–1235, Dec. 2005, doi: [10.1109/JMEMS.2005.859089](https://doi.org/10.1109/JMEMS.2005.859089).

[20]

Z. Gao and D. Zhang, “Design, analysis and fabrication of a multidimensional acceleration sensor based on fully decoupled compliant parallel mechanism,” *Sensors and Actuators A: Physical*, vol. 163, no. 1, pp. 418–427, Sep. 2010, doi: [10.1016/j.sna.2010.08.021](https://doi.org/10.1016/j.sna.2010.08.021).

[21]

B. G. Winder, S. P. Magleby, and L. L. Howell, “A Study of Joints Suitable for Lamina Emergent Mechanisms,” Jul. 2009, pp. 339–349. doi: [10.1115/DETC2008-49914](https://doi.org/10.1115/DETC2008-49914).

[22]

T. J. Teo, G. Yang, and I.-M. Chen, “A large deflection and high payload flexure-based parallel manipulator for UV nanoimprint lithography: Part I. Modeling and analyses,” *Precision Engineering*, vol. 38, no. 4, pp. 861–871, Oct. 2014, doi: [10.1016/j.precisioneng.2014.05.003](https://doi.org/10.1016/j.precisioneng.2014.05.003).

[23]

N. T. Pavlović and N. D. Pavlović, “Compliant mechanism design for realizing of axial link translation,” *Mechanism and Machine Theory*, vol. 44, no. 5, pp. 1082–1091, May 2009, doi: [10.1016/j.mechmachtheory.2008.05.005](https://doi.org/10.1016/j.mechmachtheory.2008.05.005).

[24]

B. P. Trease, Y.-M. Moon, and S. Kota, “Design of Large-Displacement Compliant Joints,” *Journal of Mechanical Design*, vol. 127, no. 4, pp. 788–798, Nov. 2004, doi: [10.1115/1.1900149](https://doi.org/10.1115/1.1900149).

[25]

D. Farhadi Macheckposhti, N. Tolou, and J. L. Herder, “A Review on Compliant Joints and Rigid-Body Constant Velocity Universal Joints Toward the Design of Compliant Homokinetic Couplings,” *Journal of Mechanical Design*, vol. 137, no. 3, Mar. 2015, doi: [10.1115/1.4029318](https://doi.org/10.1115/1.4029318).

[26]

S. Farah, D. G. Anderson, and R. Langer, “Physical and mechanical properties of PLA, and their functions in widespread applications — A comprehensive review,” *Advanced Drug Delivery Reviews*, Vol. 107, pp. 367-392.

[27]

R. T. L. Ferreira, I. C. A. D. Burger, and T. A. Dutra, “Experimental characterization and micrography of 3D printed PLA and PLA reinforced with short carbon fibers,” *Composite Part B Engineering*, Vol. 124, pp. 88-100.

[28]

A. Pandzic, D. Hodzic, and A. Milovanovic, “Effect of infill type and density on tensile properties of PLA material for FDM process,” *International Symposium on Intelligent Manufacturing and Automation*, 30th.

[29]

C. Abeykoon, P. Sri-amphorn, and A. Fernando, “Optimization of fused deposition modeling parameters for improved PLA and ABS 3D printed structures,” *International Journal of Lightweight Materials and Manufacturing*, Vol. 3, pp. 284-297.